

Multiple-bounce Smith Microfacet BRDFs using the Invariance Principle

Yuang Cui*
Anhui Science and Technology
University
China
yuangcui@outlook.com

Gaole Pan*
Nanjing University of Science and
Technology
China
pangaole@njust.edu.cn

Jian Yang
Nanjing University of Science and
Technology
China
csjyang@njust.edu.cn

Lei Zhang
The Hong Kong Polytechnic
University
China
cslzhang@comp.polyu.edu.hk

Ling-Qi Yan
University of California Santa
Barbara
USA
lingqi@cs.ucsb.edu

Beibei Wang[†]
Nankai University, Nanjing
University of Science and
Technology
China
beibei.wang@njust.edu.cn

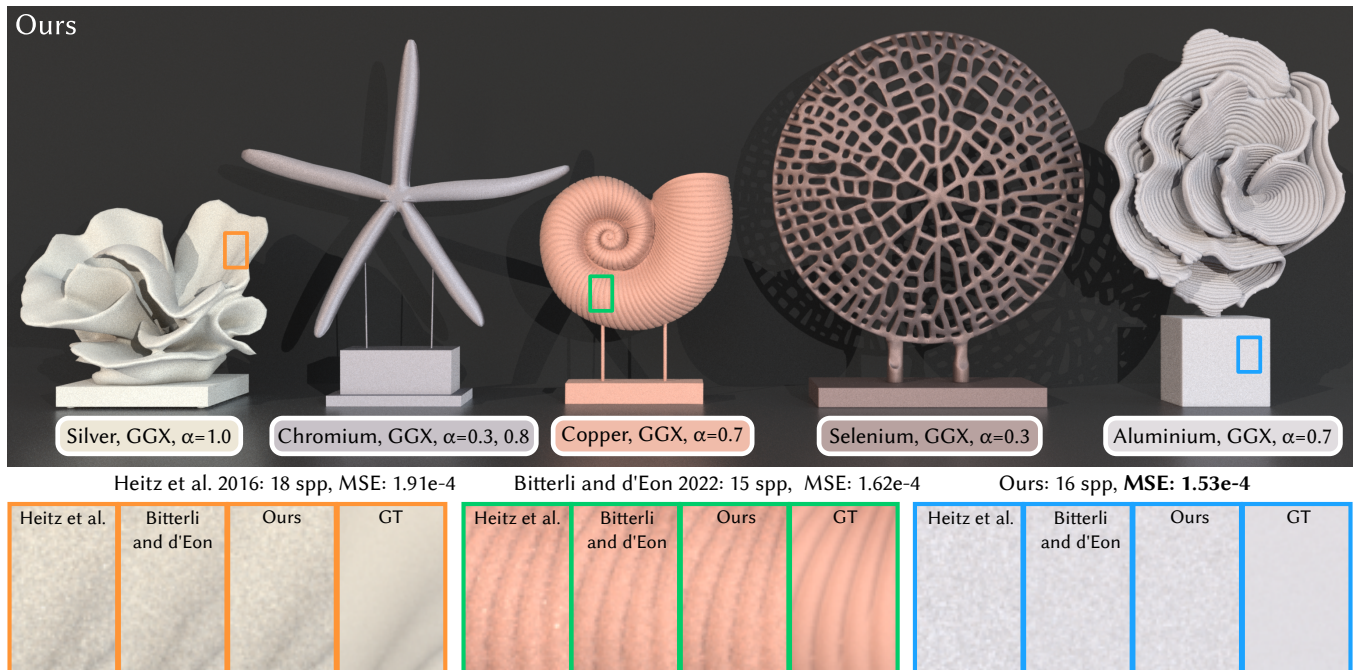


Figure 1: We propose a multiple-bounce microfacet model derived with the invariance principle. Our model produces results with less noise, compared to existing approaches (Heitz et al. [2016] and Bitterli and d'Eon [2022]), with equal time (about 11.5 seconds for point/directional lighting and 100.0 seconds for environment lighting). Note that the bidirectional reflectance distribution function (BRDF) computation by Heitz et al. [2016] is faster than others, so more samples are used for their method. Similarly, our method has a simpler formulation than Bitterli and d'Eon [2022], resulting in more samples when rendered with equal time.

*Contribute equally. Research done when Yuang Cui was an intern at Nanjing University of Science and Technology.

[†]Corresponding author.

Permission to make digital or hard copies of all or part of this work for personal or classroom use is granted without fee provided that copies are not made or distributed for profit or commercial advantage and that copies bear this notice and the full citation on the first page. Copyrights for components of this work owned by others than

ACM must be honored. Abstracting with credit is permitted. To copy otherwise, or republish, to post on servers or to redistribute to lists, requires prior specific permission and/or a fee. Request permissions from permissions@acm.org.

SA '23 Conference Papers, December 12–15, 2023, Sydney, Australia

© 2023 Association for Computing Machinery.

ACM ISBN 978-1-4503-9470-3/22/12...\$15.00

<https://doi.org/10.1145/3550469.3555380>

ABSTRACT

Smith microfacet models are widely used in computer graphics to represent materials. Traditional microfacet models do not consider the multiple bounces on microgeometries, leading to visible energy missing, especially on rough surfaces. Later, as the equivalence between the microfacets and volume has been revealed, random walk solutions have been proposed to introduce multiple bounces, but at the cost of high variance. Recently, the position-free property has been introduced into the multiple-bounce model, resulting in much less noise, but also bias or a complex derivation. In this paper, we propose a simple way to derive the multiple-bounce Smith microfacet bidirectional reflectance distribution functions (BRDFs) using the invariance principle. At the core of our model is a shadowing-masking function for a path consisting of direction collections, rather than separated bounces. Our model ensures unbiasedness and can produce less noise compared to the previous work with equal time, thanks to the simple formulation. Furthermore, we also propose a novel probability density function (PDF) for BRDF multiple importance sampling, which has a better match with the multiple-bounce BRDFs, producing less noise than previous naive approximations.

CCS CONCEPTS

• **Computing methodologies** → **Rendering; Reflectance modeling.**

ACM Reference Format:

Yuang Cui, Gaole Pan, Jian Yang, Lei Zhang, Ling-Qi Yan, and Beibei Wang. 2023. Multiple-bounce Smith Microfacet BRDFs using the Invariance Principle. In *SIGGRAPH Asia 2023 Conference Papers (SA '23 Conference Papers)*, December 12–15, 2023, Sydney, Australia. ACM, New York, NY, USA, 11 pages. <https://doi.org/10.1145/3550469.3555380>

1 INTRODUCTION

Material models are essential to realistic rendering, since they describe the interaction between light and surfaces. The microfacet model [Cook and Torrance 1982; Walter et al. 2007] is a commonly used analytical material model, which assumes that a surface is made of plenty of small microfacets. And the distribution of these microfacets, or normal distribution function (NDF), characterizes the principal appearance of the surface. Besides, the occlusion between microfacets is modeled using the shadowing-masking function, which encodes the proportion of light that may reach a microfacet without being occluded by others. Therefore, the classical microfacet bidirectional scattering distribution function (BSDF) can accurately model the *single bounce* of light among the microfacets. However, since the light can actually bounce/scatter *multiple times* before exiting the microgeometry, particularly for rough surfaces, the microfacet model can lead to an obvious energy loss.

It is difficult to solve the multiple bounces of light from the microfacet model. Various assumptions have been made, and we are especially interested in the Smith approximation – the NDFs are always the same regardless of different positions [Smith 1967]. The Smith approximation immediately suggests the similarity between microfacets and a volumetric medium, thus leading to random walk solutions by Heitz et al. [2016] and Dupuy et al. [2016].

They trace light paths inside the volume, keeping track of the positions of each bounce and producing accurate results. Bitterli and d'Eon [2022] decrease the integral dimension using a closed-form formulation of the height distribution by assuming a hyperexponential distribution, leading to unbiased and less-noisy results. Wang et al. [2022a] introduce the position-free property into the multiple-bounce computation, assuming the independence between the bounces (except sharing the same direction). Their model produces much less noise for both reflection and refraction and is unrelated to any specific height distribution. However, their results differ from the previous works due to the independent-bounce assumption.

In this paper, we propose an unbiased multiple-bounce microfacet model with the invariance principle [Ambartsumian 1943], which was introduced for planetary physics and radiative transfer by Ambartsumian [1943] for isotropic scattering and known as the Chandrasekhar's BRDF [Chandrasekhar 1960]. We extend the invariance principle to handle anisotropic phase functions, resulting in a *simple formulation* of the multiple-bounce Smith microfacet model. Thanks to this theory, we generalize the shadowing-masking function from a single bounce to an entire path built on top of the position-free multiple-bounce model by Wang et al. [2022a]. In practice, since our model has a simpler formulation, it results in an even lower noise level compared to the previous method [Bitterli and d'Eon 2022] when rendered with equal time, while retaining their merits, e.g., passing the white furnace test, and working with anisotropic materials and general normal distributions such as Beckmann [Beckmann and Spizzichino 1963] and GGX [Walter et al. 2007].

Furthermore, we improve the PDF of the multiple-bounce microfacet model by approximating the multiple bounces within a semi-infinite anisotropic medium with an isotropic multiple-bounce approximation [Hapke 1981]. Our PDF better matches the multiple-bounce function than the commonly used approximation [Heitz et al. 2016; Wang et al. 2022a] – the single-bounce microfacet model together with a Lambertian term, leading to a higher quality when rendered with multiple importance sampling (MIS) [Veach 1997], particularly for low-roughness materials where the Lambertian approximation no longer holds.

An open source implementation of our methods is available at <https://github.com/wangningbei/sourceCodeMBSRDF>.

2 RELATED WORK

In this section, we briefly review previous works related to multiple-bounce Smith microfacet model and the invariance principle.

2.1 Multiple-bounce microfacet models.

The typical microfacet models only express the single bounce on the surface microgeometry, resulting in an energy loss. We group the existing works on multiple-bounce computations into two categories: physically-based and non-physically based models.

Physically-based multiple-bounce microfacet models. The multiple bounces of the Smith model does not have an explicit formula. Monte Carlo random walk has become one necessary solution for accurate results. For that, the microfacets are treated as randomly distributed microflakes [Heitz et al. 2016] or homogeneous medium

Table 1: Notations.

Mathematical notation	
Ω	full spherical domain
Ω^+	upper spherical domain
Ω^-	lower spherical domain
$\omega_i \cdot \omega_o$	dot product
$ \omega_i \cdot \omega_o $	absolute value of the dot product
$o()$	the infinitesimal of higher order
Physical quantities used in microfacet models	
$\omega_g = (0, 0, 1)$	geometric normal
ω_m	microfacet normal
ω_i	incident direction
ω_o	outgoing direction
$\Lambda(\omega)$	the Smith Lambda function
$D(\omega_m)$	normal distribution function
$D_{\omega_i}(\omega_m)$	visible normals' distribution
$F(\omega_i, \omega_m)$	Fresnel factor
$\rho(\omega_i, \omega_o)$	multiple-bounce BSDF with the cosine term

[Dupuy et al. 2016], where Heitz et al. [2016] need a height distribution function to trace the height¹. These methods can be extended to normal-mapped surfaces [Schüssler et al. 2017] or combined with wave optics [Falster et al. 2020]. Bitterli and d'Eon [2022] decrease the integral dimension by deriving an analytical preintegration of collision distances. The key insight of their model is an explicit formulation of the height distribution as a hyperexponential distribution. Their model produces identical results as Heitz et al. [2016], with less noise level. Recently, Wang et al. [2022a] introduce the position-free property into the multiple-bounce computation, leading to significant variance reduction, by treating each bounce at the micro-scale separately. The independent bounce assumption in their model introduces bias, making their results different from Heitz et al. [2016]. Similar to these works, our model follows the position-free assumption, reducing the multiple-bounce path integral dimensions to the angular dimension only. However, we remove the independent-bounce assumption. Thanks to the invariance principle, our model has a much simpler formulation and derivation. And in practice, this leads to identical results to Bitterli and d'Eon [2022] but with even lower noise when rendered with equal time.

Different from Smith microfacet models, the V-groove models [Lee et al. 2018; Xie and Hanrahan 2018] allow for analytic solutions for multiple bounces. However, they produce shiny appearance even on rough surfaces and have singularities in the shadowing term. We do not extend further discussion on these models.

Non-physically based multiple-bounce microfacet models. Some existing methods [Bai et al. 2022; Wang et al. 2022b; Xie et al. 2019] use neural networks to represent the multiple-bounce BSDFs, avoiding the random walk during rendering at the cost of introducing bias.

¹They observed that for a couple of specific choices of height distributions (e.g., uniform distribution and Gaussian distribution), the rendered results are the same, without proof for generalization.

Some other approximate multiple-bounce models have been proposed for efficient rendering, by mixing the single scattering with an additional lobe empirically [Kulla and Conty 2017], or by scaling the single bounce results [Turquin 2019]. These methods are fast, but are less accurate.

2.2 The Invariance principle

Ambartsumian [1943] proposed the invariance principle for radiative transfer. He derived a semi-analytical formulation to model a multiple-bounce BRDF with an isotropic phase function within a semi-infinite medium. This is the first time that the invariance principle was used to model the light transport within a medium. Later, Ambartsumian [1944] extended the semi-analytical formulation for arbitrary phase functions rather than isotropic ones.

Chandrasekhar [1960] proposed a different form of the multiple-bounce function, reducing to solving equations, known as H functions. His model is also called *Chandrasekhar's BRDF* in the following works. Horak and Chandrasekhar [1961] proposed a three-term phase function with Legendre polynomials, leading to an analytical solution to the multiple bounces within a semi-infinite medium. However, the computation is highly complex, making rendering less practical. Recently, d'Eon [2021] introduced the three-term model by Horak and Chandrasekhar [1961] for a Lambertian sphere phase function. By introducing some approximations, his model becomes much more practical and achieves a faithful appearance. Pharr and Hanrahan [2000] use the invariance principle to derive the integral scattering equation for slabs of media. Note that their model still needs to sample the depth rather than angularly only, which is a key difference from ours.

Previous works cannot be applied to the multiple-bounce computation within the microfacets directly, since the phase function in this problem is anisotropic (depends on the direction). Therefore, we derive a novel scattering function specialized for our problem.

3 BACKGROUND AND OVERVIEW

In this section, we analyze the multiple-bounce Smith models related to ours, highlighting the differences between these methods. Then we provide an overview of our model.

3.1 Path formulation of multiple-bounce Smith models

Before analyzing the existing methods, we first define the notations. The light transport at any shading point s , potentially undergoing multiple bounces, is defined as a path integral for a given pair of query directions ω_i and ω_o . Thus, the query directions ω_i and ω_o construct a path space. The light path is defined differently in the existing approaches, as shown in Figure 2. Nevertheless, this light path includes two domains: a spatial domain and an angular domain. We use a set of directions to define the angular domain: $\bar{x}_a = (d_0, d_1, \dots, d_k)$. The first and last directions are aligned with the macro incident and outgoing directions of a BSDF query, i.e., $d_0 = \omega_i$ and $d_k = \omega_o$. Note that the direction of ω_i points downwards. About the spatial domain, different models have different parameterizations.

Heitz et al. [2016] treat the microfacets as a microflake volumetric model, leading to a path defined as

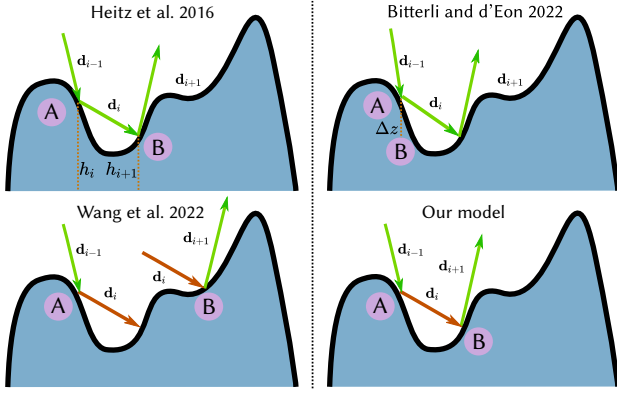


Figure 2: These four models define the path space of multiple-bounce BRDFs in different ways. The path space defined by Heitz et al. [2016] includes the height of the microgeometry. Bitterli and d’Eon [2022] turn the ray distance into the height difference and then perform preintegration on the spatial domain. Wang et al. [2022a] and our model are position-free, except our model removes the independent-bounce assumption.

$\bar{x}_H = (h_0, d_0, h_1, d_1, \dots, d_k)$. Dupuy et al. [2016] simplify the medium from anisotropic media to a homogeneous media, resulting in a path denoted as $\bar{x}_D = (d_0, t_0, d_1, t_1, \dots, d_k)$. Recently, Bitterli and d’Eon first transform the distance along a ray to a height difference Δz and then perform a preintegration of the height component; thus, the final path of their model $\bar{x}_B = (d_0, d_1, \dots, d_k)$, remains in the angular domain only. The variable change from the ray distance to the height difference allows for integrating explicitly over the depths, resulting in lower variance. All the above models provide the same result. Another model by Wang et al. [2022a] introduces the position-free property into the micro scale of a BRDF, resulting in the angular only domain directly $\bar{x}_W = (d_0, d_1, \dots, d_k)$.

3.2 Position-free multiple-bounce Smith microfacet model

Since our model is under the position-free framework by Wang et al. [2022a], we briefly review their model. Wang et al. [2022a] introduced the position-free property into the micro scale of a BRDF, resulting in a simple multiple-bounce solution for Smith microfacet models.

Starting from the light path $\bar{x} = (d_0, d_1, \dots, d_k)$, the contribution $f(\bar{x})$ of this light path is the product of vertex terms v_i (on each vertex) and segment terms s_i (on each direction):

$$f(\bar{x}) = \prod_{i=0}^{i=k-1} v_i s_i. \quad (1)$$

The vertex term v_i is defined to represent local interactions between the light and the microfacets, consisting of the normal distribution function D , the Fresnel term F , and the Jacobian term:

$$v_i = \frac{F(-d_i, \omega_h^i) D(\omega_h^i)}{4 |\omega_g \cdot (-d_i)|}, \quad (2)$$

where ω_g is the macrosurface normal and ω_h^i denotes the half vector between d_i and d_{i+1} .

The segment term considers the shadowing-masking function of the light path. Two types of shadowing-masking functions are proposed by Wang et al. [2022a]: a height-uncorrelated shadowing-masking and a height-correlated one. Both functions are defined on each bounce separately. The latter considers the correlation between incoming and outgoing rays at each bounce, while the former treats the incoming and outgoing rays at each bounce independently. The final segment terms are the accumulation of each bounce. This bounce-independent assumption leads to different rendered results from the other models.

3.3 Overview

We follow the position-free property by Wang et al. [2022a], but with one essential difference: considering the correlation of the segment term among bounces. We notice that the segment term of a bounce depends on the previous bounces. Therefore, the segment term should be defined for the entire light path rather than for individual bounces. In this way, the contribution of a light path with bounce k in our model consists of the vertex terms and a segment term S_k defined on the light path:

$$f(\bar{x}) = \left(\prod_{i=0}^{i=k-1} v_i \right) S_k(d_0, d_1, \dots, d_k), \quad (3)$$

where v_i is identical as Eqn. (2).

In the next section, we derive a segment term S_k for a light path in an elegant way using the invariance principle. Once we have the formation of S_k and thus $f(\bar{x})$ for a single light path, the final multiple-bounce BRDF can be computed similar to Wang et al. [2022a]. We just need unidirectional path tracing or bidirectional path tracing, both position-free, to sample in the path space $\bar{x}_W = (d_0, d_1, \dots, d_k)$, where each sampled light path consists of only sampled directions.

4 THE PATH SEGMENT TERM VIA THE INVARIANCE PRINCIPLE

In this section, we derive our segment term for a sampled light path using the invariance principle [Ambartsumian 1943] (Sec. 4.1). Then we analyze the main properties and merits of our model (Sec. 4.2).

The invariance principle is based on the evident but insightful fact that adding a layer of small optical thickness $\Delta\tau$ with the same properties as the original medium to this medium, should not change its reflectivity. It implies that the total contribution of the processes associated with the added layer must be zero. We follow this principle, and introduce it for medium with infinite thickness, resulting in our multiple-bounce formulation.

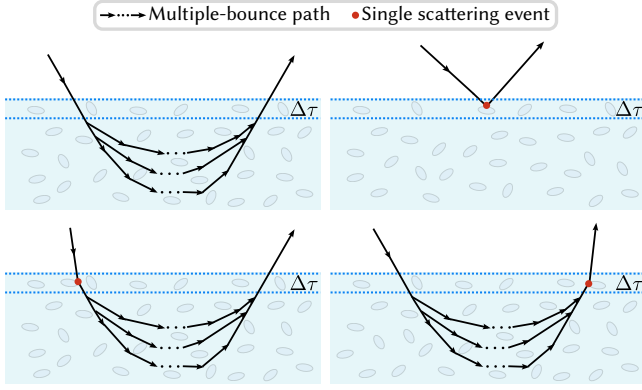


Figure 3: Four cases of light transport due to the adding of the thin layer: (a) extinction only within the thin layer; (b) scattering once within the thin layer without reaching the bottom medium ; (c) scattering at the incoming ray, and (d) scattering at the outgoing ray.

4.1 Multiple-bounce formulation for the reflective microfacet model

We follow the assumption of Dupuy et al. [2016] and Bitterli and d'Eon [2022] that the microfacet model is equivalent to a semi-infinite homogeneous medium. Given a semi-infinite homogeneous medium \mathcal{M} , we add a slice of medium with thickness $\Delta\tau$ on top of \mathcal{M} . The addition of this thin layer causes some changes in the light transport within the medium. As shown in Figure 3, we recognize four cases:

- (1) extinction within this thin layer,
- (2) scattering at thin layer without reaching the medium \mathcal{M} ,
- (3) scattering within the incoming ray when crossing the thin layer and then scattering within the medium, and leave from the outgoing ray from the thin layer without scattering, and
- (4) the symmetric case of case 3.

We only consider no scattering (case 1) or scattering once (the other three cases) in the thin layer. Since $\Delta\tau$ is chosen to be sufficiently thin, which can be at least an order of magnitude thinner than the mean free path, there is no need to consider higher-order scattering events.

CASE 1. The new added layer makes attenuation on both the incoming and the outgoing directions, leading to the following change in the outgoing radiance:

$$\begin{aligned} \Delta L_0 &= \rho(\omega_i, \omega_o) L \left(1 - e^{-\Delta\tau(|\Lambda(\omega_i)| + \Lambda(\omega_o))}\right) \\ &= \rho(\omega_i, \omega_o) (L\Delta\tau) (|\Lambda(\omega_i)| + \Lambda(\omega_o)) + o(\Delta\tau), \end{aligned} \quad (4)$$

where $\rho(\omega_i, \omega_o)$ represents the multiple-bounce BRDF with the cosine term. $L(\omega_i)$ is the incoming radiance, written as L for clarity. When x is small enough (but still a positive number), $1 - e^{-x}$ will converge to x . The infinitesimal of higher order is denoted by $o(\Delta\tau)$, which can be ignored. Λ is the Smith Lambda function [Heitz 2014].

CASE 2. The light is scattered only in the added layer, without reaching the medium \mathcal{M} :

$$\begin{aligned} \Delta L_1 &= f_p(\omega_i, \omega_o) L \left(1 - e^{-\Delta\tau|\Lambda(\omega_i)|}\right) e^{-\Delta\tau\Lambda(\omega_o)} \\ &= f_p(\omega_i, \omega_o) (L\Delta\tau) |\Lambda(\omega_i)| + o(\Delta\tau) \\ &= v(\omega_i, \omega_o) L\Delta\tau + o(\Delta\tau), \end{aligned} \quad (5)$$

where ΔL_1 is the change of the outgoing radiance due to the added layer. Note that e^{-x} converges to 1 for a small positive number x . The phase function f_p of the scattering, as Heitz et al. [2016], defined as:

$$f_p = \frac{F(\omega_i, \omega_h) D_{\omega_i}(\omega_h)}{4|\omega_h \cdot \omega_i|}, \quad (6)$$

where D_{ω_i} is the visible normal distribution function (VNDF). Interestingly, the product of the phase function and the $|\Lambda(\omega_i)|$ results in the vertex term of the single bounce.

CASE 3. The light is scattered once in the added layer, reaches medium \mathcal{M} , and later leaves the medium by going through the thin layer. Since the scattering direction in the added layer could be any direction in the lower-hemisphere, there is an integral on the lower-hemisphere here:

$$\begin{aligned} \Delta L_2 &= \int_{\Omega^-} f_p(\omega_i, \omega) (L\Delta\tau) |\Lambda(\omega_i)| \rho(\omega, \omega_o) d\omega + o(\Delta\tau) \\ &= L\Delta\tau \int_{\Omega^-} v(\omega_i, \omega) \rho(\omega, \omega_o) d\omega + o(\Delta\tau). \end{aligned} \quad (7)$$

CASE 4. The symmetric case of case 3, where the scattering happens on the outgoing direction:

$$\begin{aligned} \Delta L_3 &= \int_{\Omega^+} \rho(\omega_i, \omega) (L\Delta\tau) |\Lambda(\omega)| f_p(\omega, \omega_o) d\omega + o(\Delta\tau) \\ &= L\Delta\tau \int_{\Omega^+} \rho(\omega_i, \omega) v(\omega, \omega_o) d\omega + o(\Delta\tau). \end{aligned} \quad (8)$$

The invariance principle implies that the four cases should guarantee energy conservation:

$$\Delta L_0 = \Delta L_1 + \Delta L_2 + \Delta L_3. \quad (9)$$

Then, we have

$$\begin{aligned} \rho(\omega_i, \omega_o) (L\Delta\tau) (|\Lambda(\omega_i)| + \Lambda(\omega_o)) &= v(\omega_i, \omega_o) L\Delta\tau + \\ L\Delta\tau \int_{\Omega^-} v(\omega_i, \omega) \rho(\omega, \omega_o) d\omega &+ L\Delta\tau \int_{\Omega^+} \rho(\omega_i, \omega) v(\omega, \omega_o) d\omega. \end{aligned} \quad (10)$$

By cancelling some common factors, and unifying the integral domain to the upper hemisphere, we have

$$\begin{aligned} \rho(\omega_i, \omega_o) &= \frac{1}{\Lambda(-\omega_i) + \Lambda(\omega_o) + 1} \left(v(\omega_i, \omega_o) + \right. \\ &\left. \int_{\Omega^+} \left(v(\omega_i, -\omega) \rho(-\omega, \omega_o) + \rho(\omega_i, \omega) v(\omega, \omega_o) \right) d\omega \right). \end{aligned} \quad (11)$$

Starting from the above equation, we can easily derive the contribution of a sampled light path $\vec{x}_k^0 = (d_0, d_1, \dots, d_k)$ with bounce k :

$$f(\vec{x}_k^0) = \frac{v(d_0, -d_{k-1}) f(x_k^1) + v(d_{k-1}, d_k) f(x_{k-1}^0)}{\Lambda(-d_0) + \Lambda(d_k) + 1}. \quad (12)$$

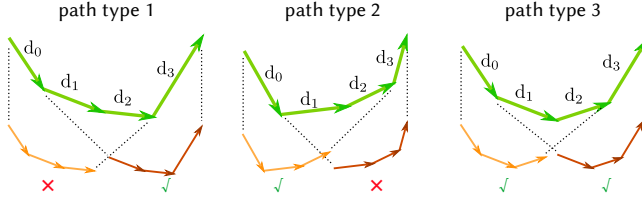


Figure 4: Three types of configurations in terms of the ray directions for a light path with three bounces. The first path type has the second recursive term in Eqn. (13) only, and the second one has the first recursive term in Eqn. (13) only, and the last path type has both recursive terms. The outgoing ray pointing downwards, or the incoming ray coming from the lower hemisphere indicates that the light path is invalid.

Substituting Eqn. (3) into the above equation and canceling the vertex terms leads to the segment term of a light path :

$$S_k(d_0, \dots, d_k) = S_1(d_0, d_k) (S_{k-1}(d_0, \dots, d_{k-1}) + S_{k-1}(d_1, \dots, d_k)). \quad (13)$$

The above equation shows that the segment term of a light path with bounce k consists of two recursive terms. However, we find that only a single recursive term has a physical meaning for some light paths. For example, in Figure 4, we show three path configurations (the orientation of the ray) for a path with three bounces. Only one recursive term exists for the first and second path types. The other recursive term in these two types has an invalid incoming/outgoing ray direction, i.e., the outgoing ray pointing downwards or the incoming ray coming from the lower hemisphere. For the last path configuration, both recursive terms exist. We also need to formulate these rules into our formulation:

$$S_1(d_0, d_1) = \frac{1}{1 + \Lambda(-d_0) + \Lambda(d_1)}, \quad (14)$$

$$S_k(d_0, \dots, d_k) = \begin{cases} 0, & \text{if } d_0.z > 0 \text{ or } d_k.z < 0, \\ S_1(d_0, d_k) (S_{k-1}(d_0, \dots, d_{k-1}) + S_{k-1}(d_1, \dots, d_k)), & \text{otherwise.} \end{cases}$$

In the above equation, we find that our single-bounce segment term ($S_1(d_0, d_1)$) also matches the height-correlated shadowing-masking function by Ross et al. [2005]. The implementation of our model is detailed in Sec. 4.3.

In theory, the time complexity of our method is $O(NM)$, where N and M represent the ray count pointing upwards and downwards respectively and $N + M = k$. Therefore, the best case of the time complexity is linear in k , and the worst case is quadratic in k . However, in practice, up to 10 bounces, the time cost is very close to a linear function of k , since most of the light paths (about 90% for Vase scene, as shown in Figure 10) only have one or two directions pointing downwards. In Figure 10, we show the segment term computation time cost curve as a function of the bounce count and provide an in-depth discussion.

Bitterli and d’Eon [2022] proposed a similar concept p_{exit} , which is the probability of a photon exiting the medium, conditioned on the directions it takes after each collision. This p_{exit} is

similar but not equivalent to our segment term, since some terms in their p_{exit} are included in our vertex term. We provide an in-depth discussion in the supplementary.

4.2 Properties and analysis

We analysis the main properties of our model in this section.

Unbiasedness and reciprocity. Our model is unbiased and produces the identical results as Heitz et al. [2016]. We provide the convergence curve of our model w.r.t. varying sample rate in Figure 10. The removal of the independent-bounce assumption from Wang et al. [2022a] makes our model unbiased. Furthermore, our model is reciprocal, since both our vertex terms and the segment term Eqn. (14) are reciprocal.

Relationship to the model by Bitterli and d’Eon [2022]. Both Bitterli and d’Eon [2022] and our model are unbiased. We also find that their model and ours are equivalent for a specific bounce (e.g., bounces = 2 or 3) with a non-trivial derivation, as shown in (Sec. 1.2) (supplementary). However, a general derivation from their model to ours for an arbitrary bounce is not apparent. Our model shows two benefits compared to theirs. First, the derivation of Bitterli and d’Eon [2022] depends on the height distribution and results in a more complex formulation, while our model has a simpler derivation thanks to the invariance principle, leading to time efficiency. Second, our model avoids singularities, which come from the minus of two Λ functions as shown in Eqn. (6) (supplementary), although the numerical stability is rarely an issue for BRDF evaluation. Hence, the rendered results of Bitterli and d’Eon [2022] have the same variance as ours with an equal number of samples, but are noisier rendered with equal time. In the supplementary, we also provide the algorithms for both models, and explicitly show the reason for our time efficiency.

4.3 Efficient BRDF evaluation and sampling

In this section, we show the implementation details of the two key components for a BRDF: evaluation and sample.

Evaluation. We provide two estimators for BRDF evaluation: a unidirectional estimator using path tracing and a bidirectional estimator using bidirectional path tracing. We provide the details for the unidirectional estimator only, and the bidirectional version is the same as Wang et al. [2022a], except for the segment term.

Starting from the incoming ray direction d_0 , we sample the visible normal distribution function to get a new direction and perform the next event estimation by connecting with the outgoing direction d_k . The path sampling termination is controlled by the Russian roulette [Arvo and Kirk 1990]. To compute S_k efficiently, we use dynamic programming, as shown in Alg. 1 (supplementary).

Sample. At each bounce, we sample the VNDF to get the outgoing direction and then compute the masking function (G_1 function) of the sampled ray to decide whether to exit the microgeometry. Otherwise, we treat the sampled direction as the incoming direction and continue sampling until the ray leaves the surface. After

getting such a light path, we compute the path contribution by evaluating the light path divided by the PDF of the sampled path.

4.4 Improved PDF for multiple-bounce BRDF

The PDF of a multiple-bounce BRDF is important for multiple importance sampling. Since no analytical formulation exists for multiple-bounce BRDFs, the previous works [Heitz et al. 2016; Wang et al. 2022a] estimate the multiple-bounce PDF with a Lambertian term and a single-bounce function, which can fit the actual multiple-bounce BRDFs well for high-roughness materials, but tends to overestimate the PDF at grazing angle directions for low-roughness BRDFs.

Our key insight is that although an anisotropic medium has no analytical multiple-bounce formulation, it can be estimated by an isotropic multiple-bounce formulation derived by Hapke [1981]:

$$f_{\text{mul}}(\omega_i, \omega_o) = \frac{a}{4\pi} \frac{H(|\omega_g \cdot \omega_i|) H(|\omega_g \cdot \omega_o|) - 1}{|\omega_g \cdot \omega_i| + |\omega_g \cdot \omega_o|}, \quad (15)$$

$$H(\mu) = \frac{1 + 2\mu}{1 + 2\sqrt{1 - a\mu}},$$

where a is the albedo of the medium.

We construct such an isotropic medium from the microfacet, by setting the albedo of the medium as $a = \frac{\alpha_x + \alpha_y}{2}$. Note that this mapping is empirical, due to the observation that the albedo of the medium dominates the scattering distribution for an isotropic medium and the roughness dominates the scattering distribution for the microfacet model. Our final PDF includes the single bounce term and the estimated multiple bounce term:

$$f_{\text{PDF}}(\omega_i, \omega_o) = \frac{D_{\omega_i}(\omega_h)}{4|\omega_h \cdot \omega_i|} + f_{\text{mul}}(\omega_i, \omega_o). \quad (16)$$

5 RESULTS

We have implemented our algorithm inside the Mitsuba renderer [2010]. The implementations of Heitz et al. [2016] and Wang et al. [2022a] are from the authors' websites. We use the height-correlated version of Wang et al. [2022a]. We also reimplemented Bitterli and d'Eon [2022] (PT). We did not provide the results of Bitterli and d'Eon [2022] (BDPT), since we were not able to reimplement their model with their provided algorithm. A detailed discussion is shown in the supplementary. For the ground truth images in Figures 1, 6 and 9, we refer to the converged results using Heitz et al. [2016]. We use MSE to measure the difference between each method and the ground truth. All timings in this section are measured on a 2.20GHz Intel i7 (48 cores) with 32 GB of main memory.

5.1 Comparisons

In Figure 5, we compare the mean BRDF reflectance and the inverse efficiency as a function of the outgoing direction for a given incoming direction over several approaches, including our method, Wang et al. [2022a], Heitz et al. [2016], and Bitterli and d'Eon [2022]. The inverse efficiency means the product of the variance and time cost, and a lower value indicates a higher quality. We

show two roughnesses ($\alpha = 0.5$ and 1.0) and two incoming directions. Our BRDF value can match both Heitz et al. [2016] and Bitterli and d'Eon [2022], while our method is the most efficient in all cases (varying roughness or different incoming directions). Wang et al. [2022a] cannot match the ground truth and introduce bias due to the independent-bounce assumption, although their model has higher performance than ours, when $\theta_o = 0$ for $\alpha = 1.0$.

Matpreview scene. In Figure 6, we show a copper Matpreview scene (GGX model, $\alpha = 1.0$) lit by a directional light. We compare our models (PT and BDPT), Wang et al. [2022a] (PT and BDPT) and Bitterli and d'Eon [2022] (PT) with equal sampling rate (4 sample per pixel (spp)). Our model (BDPT) outperforms the other methods with a slightly longer time. The result of Bitterli and d'Eon [2022] has the same variance as ours (PT) with an equal sampling rate, but has a higher time cost due to the complex formulation. Wang et al. [2022a] produce results with a low noise level, but with higher variance, since their model is biased. We also provide the difference images, which clearly show that ours (BDPT) has the lowest error.

In Figure 10, we show the MSE curve in terms of sampling rate for our methods (BDPT and PT), Heitz et al. [2016] and Wang et al. [2022a] on the Matpreview scene. The ground truth is the converged result of Heitz et al. [2016]. Our methods (BDPT and PT) can converge to the reference, which indicates that our model is unbiased. On the contrary, the model by Wang et al. [2022a] is biased due to the independent-bounce assumption. Our BDPT version has the fastest convergence compared to the others.

Vase scene. Figure 9 shows three statues (copper (GGX, $\alpha = 0.1$), aluminum (Beckmann, $\alpha = 0.6$), and gold (GGX, $\alpha = 0.5$)) on a diffuse floor with direct lighting only, lit by an environment map and a point light. We use 256 spp for the environment map lighting to better show the effect of the BRDF evaluation. To achieve equal time, we use 17 spp for our method, 34 spp for Heitz et al. [2016] and 23 spp for Wang et al. [2022a] for the point light source. The rendered result by Heitz et al. [2016] has the highest noise level. Although Wang et al. [2022a] has a similar variance as ours, their result has a larger error because of the fundamental bias.

DecorativeSet scene. We also provide a DecorativeSet scene with several statues in Figure 1, including different roughness as shown in the figure. In this scene, the statues are lit by an environment map, a directional light, and a point light, considering both direct lighting and indirect lighting. We compare our method against other two methods (Heitz et al. [2016] and Bitterli and d'Eon [2022]) with equal time and use the unidirectional estimator for all the methods. Since the BRDF sample is not mentioned in Bitterli and d'Eon [2022] and the source code is not available, we use the same BRDF sample as Heitz et al. [2016]. We use 128 spp for the environment map lighting to better show the effect of the BRDF evaluation. To achieve equal time, the sampling rates are set differently for different methods. Our method outperforms the other methods visually and quantitatively for all the settings.

Pot scene. We validate the impact of our improved PDF by showing PDF curves in Figure 8 and rendered results in Figure 7, comparing with the approximation (single bounce + the Lambertian

term) by previous work [Heitz et al. 2016; Wang et al. 2022a]. Figure 7 shows three aluminium pots of different roughnesses ($\alpha = 0.15$, $\alpha = 0.2$ and $\alpha = 0.1$) with direct lighting from environment map. We use our BRDF evaluation and sample for both results and only differ in the PDF function. By comparison, our PDF produces less noise than the previous approximation.

5.2 Performance analysis

In Figure 10, we show the time cost of the *segment term computation* w.r.t. the bounce count. We find that the time cost is almost linear as the bounce count, although our model has quadratic time complexity in theory. The time cost depends on the ray counts, which point upwards and downwards. We find that only a tiny fraction of the cases have almost even downward and upwards ray counts (as shown in the right curve) when the time complexity is high. This explains that the actual time cost is almost linear, although the theory time complexity is quadratic.

5.3 Discussion and limitations

We introduce the invariance principle in the multiple-bounce microfacet model. Unfortunately, our formulation is only derived for the spatial domain. Like any other existing work in this line of research, a Monte carlo estimator is still required for the angular domain to get a path.

Introducing the invariance principle to the multiple bounces of a refractive surface is much more complex than the reflective case. Our model relies on the equivalence between the microfacet and a homogeneous medium. However, a well-known problem is that for a refractive surface, this equivalence leads to a discontinuous mapping in the spatial domain. For the same reason, Bitterli and d'Eon [2022] also consider reflective surfaces only.

6 CONCLUSION

In this paper, we present a multiple-bounce BRDF model. Theoretically, we introduce a novel way – the invariance principle, to derive a multiple-bounce BRDF; practically, we propose an analytical formulation for the segment term for a path, resulting in unbiased results and faster convergence compared to existing models. Furthermore, we also propose a novel PDF for BRDF multiple importance sampling, allowing for a better match with the multiple-bounce BRDFs, producing less noise than commonly used approximations.

To our best knowledge, our model is the first to use the invariance principle with an anisotropic phase function. By introducing the invariance principle to the multiple-bounce microfacet, we have acquired a simple derivation and a simple form. And we believe the invariance principle can be applied to similar problems, like the layered microflake (SpongeCake) model [Wang et al. 2022b]. Furthermore, the multiple bounces of a refractive surface is challenging, but is also important as future work for a complete understanding of the microfacet theory.

ACKNOWLEDGMENTS

We thank the reviewers for the valuable comments. This work has been partially supported by the National Key R&D Program of

China under grant No. 2022ZD0116305 and National Natural Science Foundation of China under grant No. 62172220.

REFERENCES

- V. A. Ambartsumian. 1943. The problem of diffuse reflection of light by a turbid medium. *Dokl. Akad. Nauk SSSR* 19 (1943), 30–41.
- V. A. Ambartsumian. 1944. On the problem of diffuse reflection of light. *Journal of Physics* 8, 2 (1944), 65–75.
- J. R. Arvo and D. S. Kirk. 1990. Particle transport and image synthesis. *ACM SIGGRAPH Computer Graphics* (1990).
- Yaoyi Bai, Songyin Wu, Zheng Zeng, Beibei Wang, and Ling-Qi Yan. 2022. BSDF Importance Baking: A Lightweight Neural Solution to Importance Sampling Parametric BSDFs. <https://doi.org/10.48550/ARXIV.2210.13681>
- P. Beckmann and A. Spizzichino. 1963. *The scattering of electromagnetic waves from rough surfaces*. Pergamon Press.
- Benedikt Bitterli and Eugene d'Eon. 2022. A Position-Free Path Integral for Homogeneous Slabs and Multiple Scattering on Smith Microfacets. *Computer Graphics Forum* 41, 4 (2022), 93–104. <https://doi.org/10.1111/cgf.14589>
- S. Chandrasekhar. 1960. *Radiative Transfer*. Dover.
- Robert L. Cook and Kenneth E. Torrance. 1982. A Reflectance Model for Computer Graphics. *ACM Trans. Graph.* 1, 1 (Jan. 1982), 7–24.
- Eugene d'Eon. 2021. An analytic BRDF for materials with spherical Lambertian scatterers. In *Computer Graphics Forum*, Vol. 40. Wiley Online Library, 153–161.
- Jonathan Dupuy, Eric Heitz, and Eugene d'Eon. 2016. Additional Progress Towards the Unification of Microfacet and Microflake Theories. In *EGSR - Experimental Ideas & Implementations*. The Eurographics Association, 55–63.
- V. Falster, A. Jarabo, and J. R. Frisvad. 2020. Computing the Bidirectional Scattering of a Microstructure Using Scalar Diffraction Theory and Path Tracing. *Computer Graphics Forum* 39, 7 (2020), 231–242.
- Bruce Hapke. 1981. Bidirectional reflectance spectroscopy: 1. Theory. *Journal of Geophysical Research: Solid Earth* 86, B4 (1981), 3039–3054.
- Eric Heitz. 2014. Understanding the Masking-Shadowing Function in Microfacet-Based BRDFs. *Journal of Computer Graphics Techniques (JCGT)* 3, 2 (30 June 2014), 48–107. <http://jcgt.org/published/0003/02/03/>
- Eric Heitz, Johannes Hanika, Eugene d'Eon, and Carsten Dachsbacher. 2016. Multiple-Scattering Microfacet BSDFs with the Smith Model. *ACM Trans. Graph.* 35, 4, Article 58 (July 2016), 14 pages.
- Henry G. Horak and S. Chandrasekhar. 1961. Diffuse Reflection by a Semi-Infinite Atmosphere. 134 (July 1961), 45. <https://doi.org/10.1086/147126>
- Wenzel Jakob. 2010. Mitsuba renderer. <http://www.mitsuba-renderer.org>.
- Christopher Kulla and Alejandro Conty. 2017. Physically Based Shading in Theory and Practice - Revisiting Physically Based Shading at Imageworks. <http://blog.selfshadow.com/publications/s2017-shading-course/>.
- Joo Lee, Adrián Jarabo, Daniel Jeon, Diego Gutiérrez, and Min Kim. 2018. Practical multiple scattering for rough surfaces. *ACM Trans. Graph.* 37, Article 175 (Dec. 2018), 12 pages.
- Matt Pharr and Pat Hanrahan. 2000. Monte Carlo Evaluation of Non-Linear Scattering Equations for Subsurface Reflection. In *Proceedings of the 27th Annual Conference on Computer Graphics and Interactive Techniques*. ACM Press/Addison-Wesley Publishing Co., USA, 75–84. <https://doi.org/10.1145/344779.344824>
- Vincent Ross, Denis Dion, and Guy Potvin. 2005. Detailed analytical approach to the Gaussian surface bidirectional reflectance distribution function specular component applied to the sea surface. *J. Opt. Soc. Am. A* 22, 11 (Nov. 2005), 2442–2453.
- Vincent Schüssler, Eric Heitz, Johannes Hanika, and Carsten Dachsbacher. 2017. Microfacet-Based Normal Mapping for Robust Monte Carlo Path Tracing. *ACM Trans. Graph.* 36, 6, Article 205 (2017), 12 pages.
- B. Smith. 1967. Geometrical shadowing of a random rough surface. *IEEE Transactions on Antennas and Propagation* 15, 5 (1967), 668–671.
- Emmanuel Turquin. 2019. Practical multiple scattering compensation for microfacet models. https://blog.selfshadow.com/publications/turquin/ms_comp_final.pdf.
- Eric Veach. 1997. *Robust Monte Carlo Methods for Light Transport Simulation*. Ph.D. Dissertation, Stanford University.
- Bruce Walter, Stephen R. Marschner, Hongsong Li, and Kenneth E. Torrance. 2007. Microfacet Models for Refraction through Rough Surfaces. In *Rendering Techniques (proc. EGSR 2007)*. The Eurographics Association, 195–206.
- Beibei Wang, Wenhua Jin, Jiahui Fan, Jian Yang, Nicolas Holzschuch, and Ling-Qi Yan. 2022a. Position-Free Multiple-Bounce Computations for Smith Microfacet BSDFs. *ACM Trans. Graph.* 41, 4, Article 134 (jul 2022), 14 pages.
- Beibei Wang, Wenhua Jin, Miloš Hašan, and Ling-Qi Yan. 2022b. SpongeCake: A Layered Microflake Surface Appearance Model. *ACM Trans. Graph.* 42, 1, Article 8 (sep 2022), 16 pages. <https://doi.org/10.1145/3546940>
- Feng Xie and Pat Hanrahan. 2018. Multiple Scattering from Distributions of Specular V-Grooves. *ACM Trans. Graph.* 37, 6, Article 276 (2018), 14 pages.
- Feng Xie, Anton Kaplanyan, Warren Hunt, and Pat Hanrahan. 2019. Multiple Scattering Using Machine Learning. In *ACM SIGGRAPH 2019 Talks*. Article 70, 2 pages.

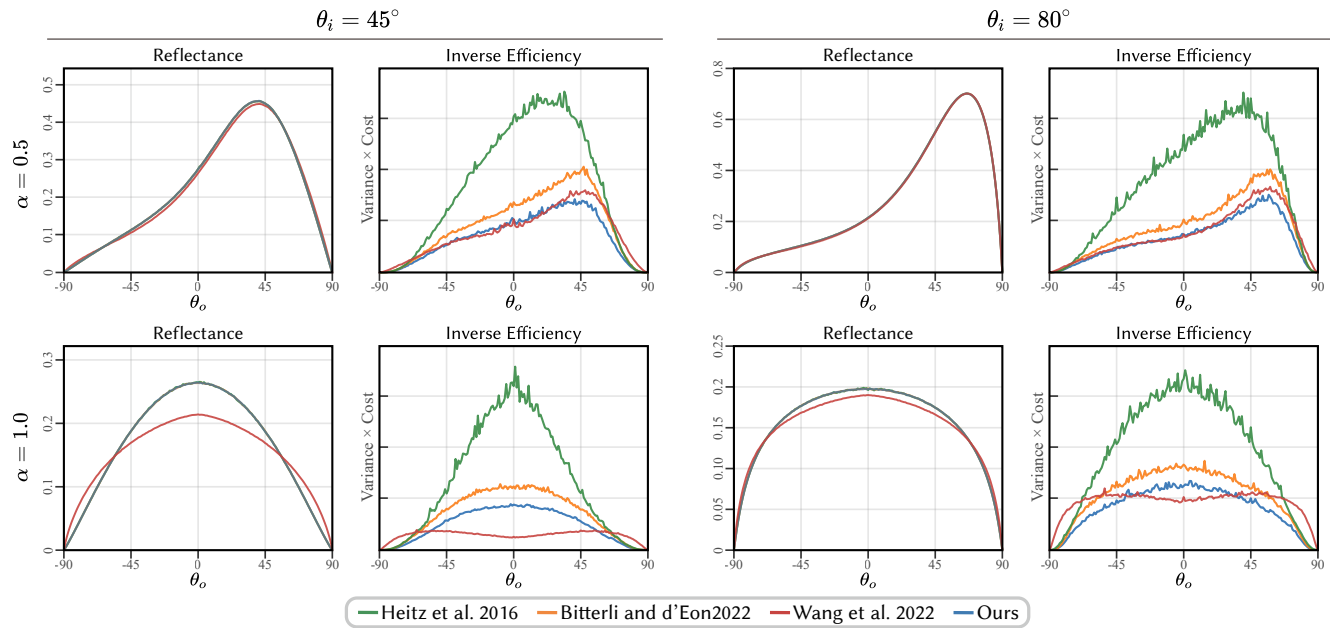


Figure 5: Comparison between our model (PT), Heitz et al. [2016], Wang et al. [2022a] (PT), and Bitterli and d’Eon [2022] (PT) in terms of BRDF reflectance and inverse efficiency (variance \times the time cost) for the rough conductor with roughness 0.5 and 1.0. Note that we use the unidirectional estimator for all models. Here, we visualize both terms as a function of the outgoing direction, given an incoming direction. θ_i and θ_o are the angles between the incident/exit directions and the normal to the macrosurface, respectively. Our BRDF value can match both Heitz et al. [2016] and Bitterli and d’Eon [2022], while our method is the most efficient in all cases (varying roughness or different incoming directions). Wang et al. [2022a] can not match the groundtruth and introduces bias due to the independent-bounce assumption, although their model has higher performance than ours, when $\theta_o = 0$ for $\alpha = 1.0$.

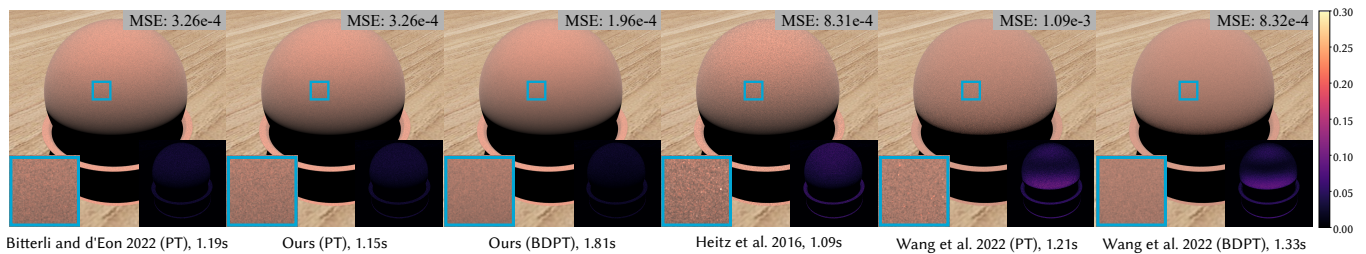


Figure 6: Comparison between our models (PT and BDPT), Wang et al. [2022a] (PT and BDPT) and Bitterli and d’Eon [2022] (PT) with equal sampling rate (4 spp) on the Matpreview scene. Our model (BDPT) produces the highest quality. Note that the model by Bitterli and d’Eon [2022] has the same variance as ours (PT) with an equal sampling rate, but has a higher time cost. The result of Wang et al. [2022a] (BDPT) has a low noise level, but shows a larger error than Heitz et al. [2016], for the reason of bias. The difference images are shown on the bottom right of each image.

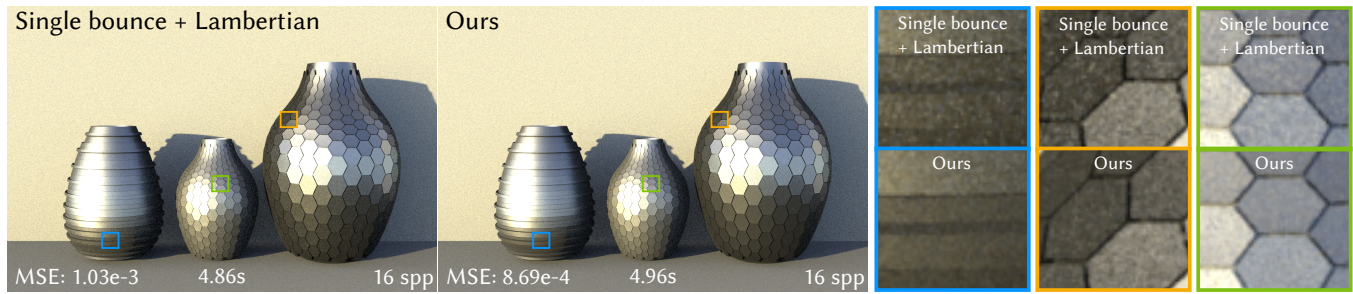


Figure 7: Comparison between our MIS PDF and single bounce + the Lambertian term (Heitz et al. [2016]) with equal sampling rate (16 spp) on the Pot scene (aluminium, $\alpha = 0.15$, $\alpha = 0.2$ and $\alpha = 0.1$). We use the same BRDF evaluation and sample in both results, and the only difference is the PDF used for MIS.

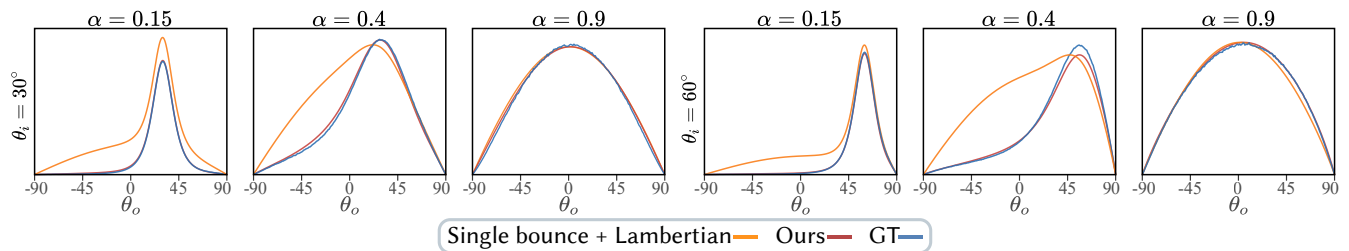


Figure 8: Comparison between our improved MIS PDF, the previous solution (single bounce + the Lambertian term) by Heitz et al. [2016] and the ground truth using the multiple-bounce BRDF reflectance. The ground truth is plotted with a stochastic aggregate of multiple-bounce BRDF with 100K samples. Our PDF matches the ground-truth PDF at all roughness, while the other solution [Heitz et al. 2016] only fits well at high roughness.

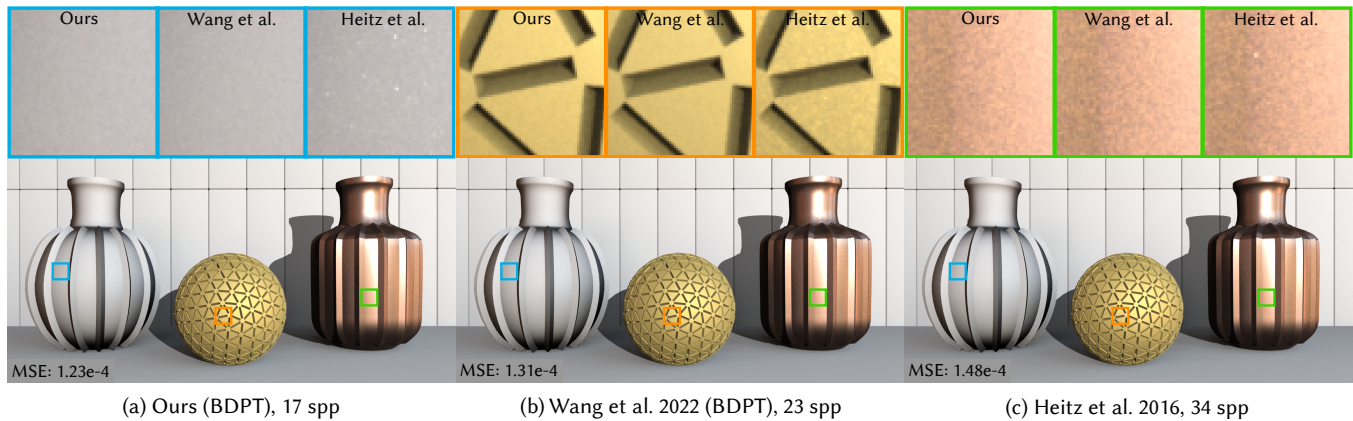


Figure 9: Equal-time comparison (about 2.8 seconds) between our model (BDPT), Wang et al. [2022a] (BDPT) and Heitz et al. [2016] on the Vase scene. Our model produces the highest quality with equal time.

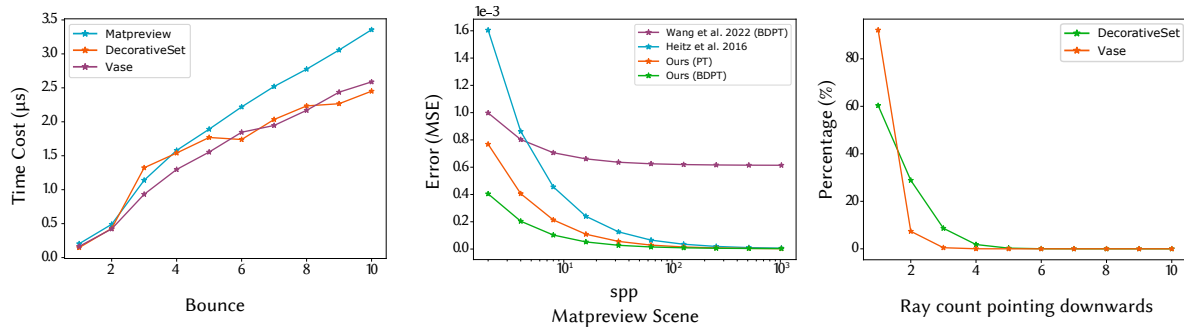


Figure 10: Left: The time cost of segment term evaluation as a function of the bounce count. Note that the time cost is almost linear to bounce. Middle: The error (MSE) of our methods (both BDPT and PT), Wang et al. [2022a] and Heitz et al. [2016] over varying sampling rate on the Matpreview scene (Figure 6). The converged result by Heitz et al. [2016] is treated as the ground truth. Our models can converge to the ground truth, while the model by Wang et al. [2022a] is biased. Both our models converge faster than Heitz et al. [2016], while the convergence rate of our model (BDPT) is the fastest. Right: The percentage of light paths as a function of the ray count pointing downwards on the Vase and DecorativeSet scenes.